Fully Coupled Implicit Method for Thermochemical Nonequilibrium Air at Suborbital Flight Speeds

Chul Park*
NASA Ames Research Center, Moffett Field, California
and
Seokkwan Yoon†
MCAT Institute, Moffett Field, California

A computational fluid dynamics (CFD) technique is described in which the finite-rate chemistry in thermal and chemical nonequilibrium air is fully and implicitly coupled with the fluid motion. Developed for use in the suborbital hypersonic flight speed range, the method accounts for the nonequilibrium vibrational and electronic excitation and dissociation but not ionization. The steady-state solution to the resulting system of equations is obtained by using a lower-upper factorization and symmetric Gauss-Seidel sweeping technique through Newton iteration. Inversion of the left-hand-side matrices is replaced by scalar multiplications through the use of the diagonal dominance algorithm. The code, named compressible Euler-Navier-Stokes two-dimensional hypersonic (CENS2H), is fully vectorized and requires about 8.8×10^{-5} s per node point per iteration in a Cray X-MP computer. Converged solutions are obtained after about 700 iterations. Sample calculations are made for a circular cylinder and a 10% airfoil at a 10-deg angle of attack. The calculated cylinder flowfield agrees with that obtained experimentally. The code predicts a 10% change in lift and drag and a 20% change in pitching moment for the airfoil caused by the thermochemical phenomena.

Nomenclature

A = Jacobian of the x or ξ component of the inviscid flux
A_{ij} = a coefficient in the vibrational relaxation time expression, Eq. (10)
a_i = coefficients in equilibrium-constant expression, Eq. (19)
B = Jacobian of the y or η component of the inviscid flux
B_{ij} = a coefficient in the vibrational relaxation time expression, Eq. (10)
C_{ki} = rate constant for reaction k with species i as the third body, $m^3mole^{-1}s^{-1}$, Eq. (17)
D_ξ = difference operator along ξ
D_η = difference operator along η
E = energy per unit volume, J/m^3
E_e = electronic excitation energy, J/m^3
E_v = vibrational energy, J/m^3
F = x or ξ component of the inviscid flux
F_v = x or ξ component of the viscous flux
G = y or η component of the inviscid flux
G_v = y or η component of the viscous flux
H = Jacobian of the chemical source S
h_{0i} = energy of formation of species i at 0K, J/mole
I = unit matrix
i = grid index along ξ (along body surface)
i = species index: 1 = O, 2 = N, 3 = NO, 4 = O_2, 5 = N_2
j = grid index along η (normal to body surface)
K_e = equilibrium constant, Eq. (19)
k = reaction index
k_{fki} = forward (endothermic) reaction rate coefficient for reaction k involving species i as the third body
k_{rki} = reverse (exothermic) reaction rate coefficient for reaction k involving species i as the third body
M_i = molecular weight of species i, kg/mole
m = average mass of the gas mixture, kg/particle
n_{ki} = pre-exponential power on temperature in rate coefficient for reaction k with species i as the third body, Eq. (17)
n_i = number density of species i, $mole/m^3$
p = pressure, Pa or atm
Q = conserved variable
q_x = heat transfer rate in the x direction
q_{vex} = heat transfer rate of the vibrational-electronic mode in the x direction
R = right-hand-side residual
S = thermochemical source
$\mathbb{S}$ = a characteristic exponent in Eq. (9)
T = translational-rotational temperature, K
T_d = characteristic temperature of reaction, K
T_v = vibrational-electronic temperature, K
t = time, s
u = x or ξ component of velocity
u^d = x or ξ component of diffusion velocity
v = y or η component of velocity
v^d = y or η component of diffusion velocity
W_e = strength of the chemical source for electronic energy, $J/(m^3s)$
W_i = strength of chemical source of species i, $kg/(m^3s)$
W_{ki} = rate of chemical reaction k involving species i as the third body, $mole/(m^3s)$
W_v = strength of the chemical source for vibrational energy, $J/(m^3s)$
w_{ij} = rate of change of vibrational energy of species i by the collisions of species j, J/(mole-s)
x = horizontal coordinate, m
y = vertical coordinate, m
ϵ_{ei} = electronic excitation energy of species i, J/mole

Presented as Paper 89-1974 at the AIAA 9th Computational Fluid Dynamics Conference, Buffalo, NY, June 14-16, 1989; received Sept. 1, 1989; revision received Feb. 13, 1990.

*Head, Experimental Aerothermodynamics Section. Associate Fellow AIAA.
†Senior Scientist. Member AIAA.

ϵ_{vi} = vibrational excitation energy of species i, J/mole
ρ = density, kg/m^3
ρ_i = density of species i, kg/m^3
τ_c = collision-limited vibrational relaxation time, s
τ_{Lij} = vibrational relaxation time in Landau-Teller expression given by Millikan and White, for molecule i in collision with species j, s
τ_{xy} = x component of the viscous stress in the y plane
ξ = curvilinear coordinate along body surface
η = curvilinear coordinate normal to body surface

Introduction

THE effects of finite-rate nonequilibrium thermochemical phenomena have been studied initially for the purpose of calculating the convective heat transfer rates to a low-catalytic wall of a re-entry vehicle such as the Space Shuttle Orbiter. Because a low-catalytic wall rejects the heat of surface recombination of atomic oxygen, the concentration of atomic oxygen in the flow affects the convective heat transfer rates. More recently, the nonequilibrium phenomena have been calculated for the purpose of determining radiative heat transfer rates (e.g., Ref. 1) and electron densities in the shock layer over the entry vehicles (e.g., Ref. 2).

The main purpose of any computation fluid dynamics (CFD) calculation is to determine forces, moments, and heat transfer rates. For the purpose of determining heat transfer rates, one must know first the extent of dissociation of oxygen and nitrogen molecules for the reason given above and second the radiative transfer rates if it is significant. At suborbital flight speeds in the Earth's atmosphere, that is, at speeds below about 8 km/s, radiation is negligible, and so only the dissociation needs to be studied. The effects of thermochemical nonequilibrium on forces and moments at hypersonic flight speeds have not been studied until very recently. Vibrational and electronic excitation, dissociation, and ionization process all absorb energy and thereby cause the temperature to be lower than in a perfect gas. This may occur either behind a shock wave, when the shock angle is steep, or in the boundary layer via the viscous dissipation (recovery phenomenon), when the inviscid flow over the boundary layer is hypersonic. The decrease in temperature accompanies a rise in density. The rise in density in turn causes the shock layers around hypersonic vehicles to be thinner than in a perfect gas. For an airfoil inclined at a finite angle of attack, a thinner shock layer leads to a smaller shock angle. This in turn leads to a lower pressure on the body surface resulting in a change in lift, drag, and pitching moment.

In Ref. 3, we have introduced a computer code, named compressible Euler-Navier-Stokes two-dimensional hypersonic (CENS2H), that calculates the finite-rate thermochemical nonequilibrium processes in such a flow regime. This code was run for an Apollo-shaped, two-dimensional, blunt-body geometry in Ref. 3 for the purpose of determining the pitching moment and trim angle of attack. It was shown therein that the pitching moment is affected significantly by the chemical reactions and that the observed shift in the trim angle of attack of the Apollo vehicle during its entry flight can be attributed to the nonequilibrium phenomena.

The CENS2H uses a two-temperature model in which the nonequilibrium vibrational temperature is calculated simultaneously with the dissociation processes. The usefulness of this model has been demonstrated in Refs. 1, 3, and 4. In Refs. 2 and 5, Candler used a multitemperature model in which the vibrational temperatures of each molecular species and electron temperature are all calculated independently. However, as Refs. 2 and 5 show, the vibrational temperatures of the different molecular species and the electron temperature are nearly the same because of the fast transfer of the vibrational energies among the different molecules and between the vibrational and electron translational modes. Therefore, the two-temperature model in Refs. 1, 3, and 4 and the multitemperature model in Refs. 2 and 5 can be considered to be equivalent. By comparing the calculations with the experimental data given in Ref. 6, Ref. 5 shows that the shock standoff distance and density distribution behind the shock over a two-dimensional circular cylinder can be calculated accurately only by using the multitemperature model.

The purpose of the present paper is to describe the computational aspect of the CENS2H code and to present the results of computation for two flow geometries: a two-dimensional circular cylinder and a two-dimensional airfoil of 10% thickness. The cylinder case calculation is made for one of the conditions experimentally tested by Hornung[6] in a shock tunnel and is one of the two such cases successfully reproduced computationally by Candler.[5] The density distribution in the shock layer over the cylinder calculated in the present work agrees with that observed in the experiment and with the work of Candler. The airfoil case is calculated in order to demonstrate the change in aerodynamic characteristics of a slender body by the thermochemical effects.

Conservation Equations

Because ionization phenomena are neglected, it leaves only the five neutral species, O, N, NO, O_2, and N_2, to be considered. Identifying these five species by the subscripts 1 through 5, and denoting the densities of these species by ρ_1 through ρ_5, the global mass conservation condition dictates

$$\rho = \sum_{i=1}^{5} \rho_i \qquad \text{kg/m}^3 \tag{1}$$

In addition, we assume that the elemental ratio between oxygen and nitrogen is conserved. This assumption is always correct in the inviscid region of the flow. In a viscous region, it is true if the diffusion coefficients of the five species are such that the net rates of elemental diffusion of the nitrogen and oxygen are the same. Diffusion rate of a species is inversely proportional to its collision cross sections and to the square root of its molecular weight. The uncertainty existing presently in the magnitudes of the cross sections is of the same order as the differences in the square roots of molecular weights among species, and, therefore, more precise formulation is not warranted. By denoting the species number density in the unit of mole/m^3 by n, and assuming the molar concentration of oxygen and nitrogen in air to be 21 and 79%, respectively, the elemental conservation condition is written as

$$\frac{n_1 + n_3 + 2n_4}{n_2 + n_3 + 2n_5} = \frac{0.21}{0.79} \tag{2}$$

Using Eqs. (1) and (2), the density and number density of O_2, ρ_4, and n_4 and those of N_2, ρ_5, and n_5 can be expressed as linear combinations of ρ, ρ_1, ρ_2, and ρ_3.

We assume that the rotational mode is in equilibrium with the translational mode and that these two modes are characterizied by the translational-rotational temperature T. This assumption is based on the knowledge, supported by many experimental data, that the equilibration between the translational and rotational modes is quite fast. We assume also that the electronic excitation mode is in equilibrium with the vibrational mode and that the two modes are characterizied by the vibrational-electronic temperature T_v. We calculate T_v independently.

In a two-dimensional flow, the conservation equations in the present system can be written in the Cartesian (x, y) coordiates in the form

$$\frac{\partial Q}{\partial t} + \frac{\partial}{\partial x}\left(F - F_v\right) + \frac{\partial}{\partial y}\left(G - G_v\right) = S \tag{3}$$

where Q signifies the conserving variables, F and G are the x and y components of the inviscid flux vectors, and F_v and G_v

are the x and y components of the viscous flux vectors. The quantity S is the thermochemical production rate (source term). The Q vector in the present work is

$$Q = \begin{bmatrix} \rho \\ \rho u \\ \rho v \\ E \\ E_v + E_e \\ \rho_1 \\ \rho_2 \\ \rho_3 \end{bmatrix} \tag{4}$$

Here, u and v are the x and y components of the velocity, and E is the energy per unit volume. E_v and E_e are vibrational electronic energies, and ρ_1, ρ_2, and ρ_3 are the densities of the species O, N, and NO. The inviscid fluxes F and G are

$$F = \begin{bmatrix} \rho u \\ \rho u^2 + p \\ \rho uv \\ u(E+p) \\ u(E_v + E_e) \\ \rho_1 u \\ \rho_2 u \\ \rho_3 u \end{bmatrix}, \quad G = \begin{bmatrix} \rho u \\ \rho uv \\ \rho v^2 + p \\ v(E+p) \\ v(E_v + E_e) \\ \rho_1 v \\ \rho_2 v \\ \rho_3 v \end{bmatrix} \tag{5}$$

The corresponding viscous flux vectors are

$$F_v = \begin{bmatrix} 0 \\ \tau_{xx} \\ \tau_{xy} \\ u\tau_{xx} + v\_\tau_{xy} - q_x \\ -q_{vex} \\ -\rho_1 u_1^d \\ -\rho_2 u_2^d \\ -\rho_3 u_3^d \end{bmatrix}, \quad G_v = \begin{bmatrix} 0 \\ \tau_{xy} \\ \tau_{yy} \\ u\tau_{xy} + v\tau_{yy} - q_y \\ -q_{vey} \\ -\rho_1 v_1^d \\ -\rho_2 v_2^d \\ -\rho_3 v_3^d \end{bmatrix} \tag{6}$$

Here q_{ve} is the rate of heat transfer in the vibrational-electronic mode.[8] The total heat transfer rate q is the sum of those due to conduction (transportation of translational-rotational energy), diffusion of chemical species (transport of reaction energies), and diffusion of vibrational-electronic excited species (transport of internal energies). The quantities u_i^d and v_i^d are the diffusion velocities of species i in the x and y directions, respectively. The full Navier-Stokes components are included in the evaluation of the F_v and G_v vectors. The flow is assumed to be laminar in the sample calculations performed in the present work. The source production term is in the form

$$S = \begin{bmatrix} 0 \\ 0 \\ 0 \\ 0 \\ W_v + W_e \\ W_1 \\ W_2 \\ W_3 \end{bmatrix} \tag{7}$$

Thermochemical Model

Vibrational Model

The vibrational energy content of the flow E_v in J/m^3 is a sum of those of the three molecules. Denoting the vibrational energy per mole of species i by ϵ_{vi},

$$E_v\left(n_i, T_v\right) = \sum_i n_i \epsilon_{vi} \qquad \text{J/m}^3 \tag{8}$$

where

$$\epsilon_{vi} = 8.314 \frac{\theta_i}{\exp[(\theta_i/T_v) - 1]} \qquad \text{J/mole}$$

θ_i being the characteristic vibrational temperature of the molecule, $\theta_i = 2740$, 2273, and 3393 K for $i = 3$, 4, and 5, respectively. The constant 8.314 represents the product of the Avogadro number and the Boltzmann constant in the MKS units.

The rate of change of average vibrational energy of the molecule i by collisions with species j is given by[1,4]

$$w_{ij} = \frac{\epsilon_{viE} - \epsilon_{vi}}{(\tau L_{ij} + \tau_c)} \left| \frac{T_s - T_v}{T_s - T_{vs}} \right|^{\mathcal{S}-1} \qquad \text{J/(mole·s)} \tag{9}$$

where ϵ_{viE} is the average vibrational energy of the species i per mole, in J/mole, evaluated as the translational temperature T. The quantity τ_{Lij} is the vibrational relaxation time according to the Landau-Teller model for molecule i by collisions with species j[7]

$$\tau_{Lij} = \exp\left(A_{ij} T^{-1/3} - B_{ij}\right)/p_c \qquad \text{s} \tag{10}$$

where p_c is the partial pressure of the colliding particles in atm. The quantity τ_c is the average collision time determined from

$$\tau_c = (c\bar{n}\sigma_v)^{-1}$$

where c is the average molecular speed $c = \sqrt{8kT/\pi m}$, m is the average mass, $\bar{n}$ is the total number density of the mixture, and σ_v is the limiting cross section. The cross section σ_v is taken to be[1]

$$\sigma_v = 10^{-21}(50{,}000/\text{T})^2 \qquad \text{m}^2$$

T_s and T_{vs} are the translational-rotational and vibrational-electronic temperatures immediately behind the shock wave, respectively. The quantity $\mathcal{S}$ is given by[1,4]

$$\mathcal{S} = 3.5 \exp(-T_s/5000)$$

The temperature T_s is taken to be the peak value of T behind the shock wave. The quantities T_s and $\mathcal{S}$ are assumed to be constant for a constant j (the spatial index normal to the body). The parameters A_{ij} and B_{ij} are given in Ref. 3. Minor changes have been made to these values in the present work in order to bring the calculated τ_{Lij} values into closer agreement with the experimentally determined values. The details are not given here because they are inconsequential for the purpose of the present paper. They will be presented in a later paper.

The rate of change of vibrational energy per unit volume of the flow W_v in J/(m^{3}s), is given by

$$W_v = \sum_i \left[\sum_j \left(n_i w_{ij} \right) - \bar{\epsilon}_i \frac{W_i}{M_i} \right] \qquad \text{J/(m}^3\text{s)} \tag{11}$$

where $\bar{\epsilon}_i$ is the average vibrational energy removed in the dissociation of molecule i. Following Refs. 1 and 4, $\bar{\epsilon}_i$ is taken to be 80% of the dissociation of molecule i: $\bar{\epsilon}_i = 0.8 \times 2 \times h_0 i$ J/mole.

The vibration model was developed for the flow behind a shock wave.[1,4] In a rapidly expanding flow or in a boundary

layer, the model is not expected to be valid. The present model tends to overpredict the vibrational relaxation time in the boundary layer. However, this is inconsequential because the boundary-layer flow tends to be frozen, and the distribution of the vibrational temperature therein is determined mainly by diffusion and conduction.

Electronic Excitation Model

The electronic excitation energy of the gas flow E_e is given by

$$E_e\left(n_i, T_v\right) = \sum_i n_i \epsilon_{ei} \qquad \text{J/m}^3 \tag{12}$$

where ϵ_{ei} is the electronic energy of the species i in the unit of J/mole. The expressions for ϵ_{ei} are given in Ref. 8. The rate of change of electronic excitation energy of the flow, W_e, is given by

$$W_e = \sum_i \epsilon_{ei} \frac{W_i}{M_i} \qquad \text{J/(m}^3\cdot\text{s)} \tag{13}$$

where W_i signifies the rate of change of the species density ρ_i by the chemical reactions to be specified below.

At each computing node point, the sum of the vibration energy E_v and the electronic energy E_e is available as a function of n_i and T_v. Since n_i is related to ρ and ρ_i, one can write

$$E_v + E_e = \text{Eq. (8)} + \text{Eq. (12)} = \text{ a function of } \rho,\ \rho_i,\ T_v \tag{14}$$

The vibrational-electronic temperature T_v is determined by solving this transcendental equation. A two-step Newtonian iteration is employed to do so.

Chemical Reaction Model

At each computing node point, the global density ρ, velocity components u and v, energy per unit volume E, the sum of vibrational and electronic energy $E_v + E_e$, and number densities n_i are available. Using these quantities, the translational-rotational temperature can be calculated by the equation

$$E = \left(\sum_i C_{vi} n_i\right) T + E_v + E_e + \sum h_{0i}\, n_i + \frac{\rho}{2}\left(u^2 + v^2\right) \qquad \text{J/m}^3 \tag{15}$$

Here C_{vi} is the frozen specific heat at constant volume for species i accounting for translational and rotational energies, in J/(mole-K), $C_{v1} = C_{v2} = 12.47$ and $C_{v3} = C_{v4} = C_{v5} = 20.79$ J/mole. The quantity h_{0i} is the energy of formation of species i, $h_{0i} = 246.81$, 470.70, 89.790, 0, and 0 kJ/mole for $i = 1$ to 5, respectively.

According to the two-temperature model, the rate coefficients are a function of the average temperature T_a, which is a geometrically averaged temperature between T and T_v defined as[1,4]

$$T_a = \sqrt{T_v T} \tag{16}$$

The endothermic reaction rate coefficient for reaction k with the third body i, k_{fki}, is given by

$$k_{fki} = C_{ki} T_a^{\,nki} \exp\left(-T_{dki}/T_a\right) \qquad \text{mole/(m}^3\text{ s)} \tag{17}$$

The rate parameters C and n used in the present work are summarized in Table 1. They are different from those used in Ref. 3 in that the N_2 dissociation reactions, reactions 8 through 12, have been included. The reaction rate coefficients are taken from Refs. 9-11 as indicated in the table. The reverse (exothermic) rates are calculated from the forward rates using the assumption that the two rates are related by the equilibrium constant evaluated at T_a, that is,

$$k_{rki} = k_{fki}/K_{ek}(T_a) \tag{18}$$

The equilibrium constants K_{ek} are determined using the partition functions calculated using the up-to-date atomic and molecular constants and are expressed in the form[1,4]

$$K_{ek} = \exp\left[a_1 z + a_2 + a_3 \ln\left(1/z\right) + a_4/z + a_4/z^2\right] \tag{19}$$

where $z = T_a/10{,}000$. The numerical values of a_is are given in Table 2.

For the purpose of comparison, calculations have been made also with the thermochemical rate parameters altered. The constant C in Eq. (17) is multiplied by 10^{-6} and the relaxation times τ_{Lij}, Eq. (10), and τ_c, Eq. (9), are multiplied by 10^6 to produce the solutions for the perfect gas. Also, while keeping the C values as given in Table 1, the vibrational relaxation times are divided by 100 in order to produce the solutions for the one-temperature relaxing gas. An equilibrium-flow solution is obtained by using the C values that are 100 times those given in the table together with the small τ values.

Numerical Method

The system of linear equations in the Cartesian coordinate system represented by Eq. (3) is converted into a curvilinear coordinate system in ξ and η. Let A and B be the Jacobian matrices of the inviscid flux vectors in the ξ-η coordinates, D_ξ and D_η difference operators that approximate $\partial/\partial\xi$ and $\partial/\partial\eta$, and δQ the correction. Then the present numerical scheme is expressed by

$$\left[I + \beta\Delta t\left(D_\xi A + D_\eta B - H\right)\right]\delta Q$$

$$= -\Delta t\left[D_\xi(F - F_v) + D_\eta(G - G_v) + S\right]$$

where I is the identity matrix, H the Jacobian matrix of the source vector S, $H = \partial S/\partial Q$, and β is 1 or ½ depending on the order of accuracy or stability chosen. The scheme is implicit for the inviscid flux and explicit for the viscous flux. With respect to the chemical reactions, the scheme is fully coupled and implicit. The first-order (in time), accurate, lower-upper symmetric Gauss-Seidel (LU-SGS) factorization

Table 1 Reaction rate parameters C_{ki}, n_{ki}, and T_{ki} in Eq. (17)

k	i	Reaction	C_k, m³/mole·s	n_k	T_{dk}, K	Ref.
1	1	$O_2+O\rightarrow O+O+O$	1.0×10^{16}	−1.5	59,500	9
2	2	$O_2+N\rightarrow O+O+N$	1.0×10^{16}	−1.5	59,500	est
3	4	$O_2+NO\rightarrow O+O+NO$	2.0×10^{15}	−1.5	59,500	est
4	4	$O_2+O_2\rightarrow O+O+O_2$	1.0×10^{16}	−1.5	59,500	9
5	5	$O_2+N_2\rightarrow O+O+N_2$	2.0×10^{15}	−1.5	59,500	est
6		$N_2+O\rightarrow NO+N$	1.8×10^{8}	0.0	76,000	10
7		$NO+O\rightarrow O_2+N$	2.2×10^{3}	1.0	19,500	11
8	1	$N_2+O\rightarrow N+N+O$	3.0×10^{16}	−1.6	113,200	est
9	2	$N_2+N\rightarrow N+N+N$	3.0×10^{16}	−1.6	113,200	9
10	3	$N_2+NO\rightarrow N+N+NO$	7.0×10^{15}	−1.6	113,200	est
11	4	$N_2+O_2\rightarrow N+N+O_2$	7.0×10^{15}	−1.6	113,200	est
12	5	$N_2+N_2\rightarrow N+N+N_2$	7.0×10^{15}	−1.6	113,200	9

Table 2 Coefficients a_i in Eq. (19)

k	a_1	a_2	a_3	a_4	a_5
1-5	0.55388	16.27551	1.77630	−6.5720	0.031445
6	0.97646	0.89043	0.74572	−3.9642	0.007123
7	0.004815	−1.7443	−1.2227	−0.95824	−0.045545
8-12	1.53510	15.4216	1.2993	−11.4940	−0.006980

scheme[12,13] can be written as

$$LD^{-1}U\delta Q = -\Delta t(R+S) \tag{20}$$

where L and U are the lower and upper operators

$$L = I + \beta\Delta t(D_\xi^- A + D_\eta^- B^+ - A^- - B^- - H)$$

$$U = I + \beta\Delta t(D_\xi^+ A^- + D_\eta^+ B^- + A^+ + B^+)$$

The matrix D is

$$D = I + \beta\Delta t(A^+ + B^+ - A^- - B^-)$$

and R is the right-hand-side (RHS) residual

$$R = D_\xi(F - F_v) + D_\eta(G - G_v) + S \tag{21}$$

Here, D_ξ^- and D_η^- are the backward difference operators and D_ξ^+ and D_η^+ are the forward difference operators. We use the central-difference operators to the unsplit inviscid fluxes in the RHS. Approximate Jacobian matrices are used in the left-hand side (LHS) to obtain a hybrid LU-SGS scheme.[12] By setting Δt to infinity, we obtain a Newton iteration form. The Jacobian matrices are approximately constructed to obtain diagonal dominance. The "+" matrices have nonnegative eigenvalues, while the "−" matrices have nonpositive eigenvalues. For example,

$$A^\pm = \tfrac{1}{2}\left[A \pm \chi(A)I\right]$$

and

$$\chi(A) = \kappa\, Max\left[|\lambda(A)|\right] \tag{22}$$

where $\lambda(A)$ represents the eigenvalues of the Jacobian matrix A, and κ is an arbitrary constant that is greater than or equal to 1.

In order to suppress the tendency for odd- and even-point decoupling and to prevent unphysical oscillations near discontinuities, a suitable dissipation model must be incorporated. If the flux-difference split dissipation model is used, one might recover Roe's upwind scheme, which is known to be accurate in most applications. However, such a fully upwind scheme was found to encounter a numerical difficulty in hypersonic flows.[13] The conventional artificial viscosity model introduces extraneous numerical errors in the hypersonic blunt-body flow also and, therefore, cannot be used. For this reason, we choose to use the flux-limited dissipation model.[13] For this purpose, the numerical flux balance of each cell for the semi-discrete scheme is written as

$$\left(F_{i+\frac{1}{2},j} - F_{i-\frac{1}{2},j} + G_{i,j+\frac{1}{2}} - G_{i,j-\frac{1}{2}}\right) - \left(d_{i+\frac{1}{2},j} - d_{i-\frac{1}{2},j} + d_{i,j+\frac{1}{2}} - d_{i,j-\frac{1}{2}}\right)$$

where d is the dissipative flux, and the indices i and j denote the computing nodes in the ξ and η directions. For simplicity, $d_{i+\frac{1}{2},j}$ is denoted by $d_{i+\frac{1}{2}}$ in the remainder of this paper. It is constructed by introducing flux limiters into the high-order terms in the form

$$d_{i+\frac{1}{2}} = -\alpha_{i+\frac{1}{2}}\left[\phi(\sigma_{i+1})e_{i+3/2} - 2e_{i+\frac{1}{2}} + \psi(\sigma_i)e_{i-\frac{1}{2}}\right]$$

where ϕ and ψ are the flux limiting functions to limit antidiffusive fluxes

$$\phi(\sigma) = \begin{pmatrix} 0 \text{ if} \sigma \le 0 \\ \sigma \text{ if } 0 \le \sigma \le 1 \\ 1 \text{ if } \sigma \ge 1 \end{pmatrix}$$

and

$$\psi(\sigma) = \phi(1/\sigma)$$

Here,

$$\sigma_i = \frac{e_i - \frac{1}{2}}{e_i + \frac{1}{2}}$$

and

$$e_{i+\frac{1}{2}} = Q_{i+1} - Q_i$$

The quantity α_i denotes

$$\alpha_{i+\frac{1}{2}} = (\kappa_0 + \kappa_1 \nu_{i+\frac{1}{2}})r(A)_{i+\frac{1}{2}} \tag{23}$$

where $r(A)$ denotes the spectral radium of matrix A. The quantity ν is the pressure sensor

$$\nu_i = \left|p_{i+1} - 2p_i + p_{i-1}\right| / (p_{i+1} + 2p_{i-1})$$

The quantities κ in Eq. (22) and κ_0 and κ_1 in Eq. (23) are initially set to large values and are reduced as the iteration progresses. The starting values are adjusted by trial and error in order to arrive at the set of values that produce the fastest converging solution. The quantity κ controls the convergence of the solution, and its magnitude does not affect the accuracy of the solution. The κ_0 and κ_1 affect the accuracy of the solution, and smaller values are preferred.

At the wall surface, the vibrational-electronic temperature T_v is assumed to be equal to the given wall temperature. The wall surfaces are assumed to be noncatalytic to chemical reactions.

The two-factor solution of δQ in Eq. (20) requires no inversion of block tridiagonal equations in the diagonally dominant scheme used here. Instead, the solution is obtained through scalar multiplications. Only the 4×4 matrix of the Jacobian of the thermochemical source S [Eq. (7)], H, needs to be inverted at each node point, the steps for which are also easily vectorized.

As mentioned in Ref. 3, the present code consumes 8.8×10^{-5} s per computing node per iteration in the Cray X-MP computer. It carries out 52.4 million floating point operations per s in the same machine. Typically, the solution for a two-dimensional flow is obtained within about 600 s.

Sample Results

Circular Cylinder in Nitrogen

The calculations are performed first for the flow around a two-dimensional circular cylinder with its axis perpendicular to the flow direction, placed in the test section of a shock tunnel. The radius of the cylinder is 2.54 cm. The freestream conditions are gas = nitrogen; density = 5.349×10^{-3} kg/m^3; velocity = 5.590 km/s; nitrogen atom mass fraction = 0.073; and temperature = 1833 K. The flow Mach number is 6.13, and the Reynolds number based on the freestream conditions and the body diameter is 24,000. The nitrogen flow is calculated using the 5-species model by setting the mole fraction of oxygen to be 10^{-6}. The calculation is initiated with a uniform parallel hypersonic flow as the starting solution.

The density distribution in the shock layer for this flow has been obtained experimentally by Hornung[6] using interferometry in a shock tunnel. The case is one of the two cases calculated by Candler.[5] The calculation by Candler was made using both a multitemperature nonequilibrium model, in which the vibrational temperatures of different molecular species are calculated independently and the electron temperature is calculated separately, and the one-temperature nonequilibrium model. Because there is only one element, nitrogen, and the

degree of ionization is negligibly small in this case, Candler's multitemperature model is virtually identical to the present two-temperature model. Two grid meshes were chosen in the present calculation: 65×39 ($= 2535$) and 65×79 ($= 5135$). The 65 points in the i direction are spread equally over the upper and lower sides of the cylinder. The constant κ in Eq. (22) was chosen to be 2 at the beginning of the iteration and was reduced down to 1.01 as iteration progressed. The quantities κ_0 and κ_1 in Eq. (23) were varied four fold in this particular calculation ($\kappa_0 = 32\kappa_1 = 0.5$, 1, or 2).

The convergence behavior of the computational method is illustrated for the case of 65×39 mesh with $\kappa_0 = 32\kappa_1 = 1$ in Fig. 1, which shows the root-mean-square (RMS) of the RHS residual R, Eq. (21), as a function of the number of iterations. As seen in the figure, the residual diminished with the number of iterations. At about 700 iterations, the residual is at least two orders of magnitude less than the initial value. The 700 iterations consume about 180 s on Cray X-MP computer for this case. At the end of 180 iterations, all flow quantities, including the surface normal gradients are nearly converged.

The results of the present calculations are compared with the interferogram[6] in Figs. 2a–2d. In these figures, the interferometric fringes have been computed using the formula given by Hornung.[6] In Fig. 2a, the calculation is carried out for a perfect gas. As seen in the figure, the calculated shock standoff distance is very much larger than the measured value. The calculated fringes have no resemblance to the experimental fringes.

In Fig. 2b, the calculation is made using the one-temperature model. As seen, the calculated standoff distance is smaller than the measured value, and the fringe pattern is different from the experimental pattern. The difference between the measured and the calculated standoff distances here is not as large as that obtained by Candler.[5] The disagreement between the two calculations is presently not explained.

In Fig. 2c, the calculation is made using the two-temperature model. As seen in the figure, the calculation reproduces both the shock standoff distance and the fringe pattern.

In Fig. 2d, the equilibrium-gas solution is shown. As seen here, the shock standoff distance calculated by the equilibrium model is significantly smaller than the measured value. The calculated fringe pattern is totally different from the experimental pattern.

In Fig. 3, the present solution obtained with the two-temperature model is compared with the solution obtained by Candler[5] using the multitemperature model. The two solutions agree quite well.

The solutions were found not to be affected by the choice of the final κ_0, κ_1 values to any discernible extent. When the mesh dimensions were changed from 65×39 to 65×79, the solution changed slightly, as shown in Fig. 4. The change is too small to affect the conclusion of the present study. No effort was made in the present work to assess the accuracy of the viscous portion of the code because no suitable experimental data could be found for this purpose.

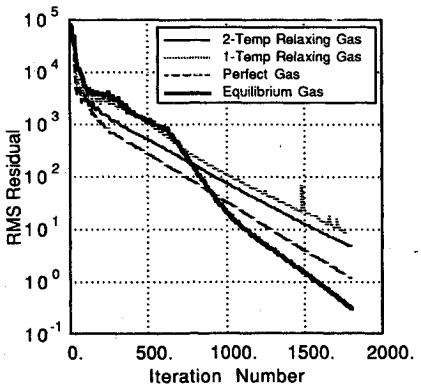

Fig. 1 Convergence history of the root-mean-square residual for the nitrogen flow over a cylinder, for the two-temperature relaxing, one-temperature relaxing, perfect-gas, and equilibrium-gas cases.

10% Airfoil at 10-deg Angle of Attack

The calculation is made next for a two-dimensional hypersonic airfoil. The airfoil is a half ellipse with a major-to-minor axis ratio of 10 to 1 and the major radius equal to the chord length. The chord length is taken to be 10 m resulting in a leading-edge radius of 10 cm. This is a typical profile of the wing of a hypersonic vehicle such as the Space Shuttle. The freestream density is chosen to be 5.608×10^{-4} kg/m^3 corresponding to an altitude of 55 km. The flight velocity is taken to be 7 km/s corresponding to a Mach number of 20.1. The angle of attack is taken to be 10 deg measured from the axis of symmetry of the ellipse. The Reynolds number based on the freestream conditions and the chord length is 2.16×10^6. The boundary layer is assumed to be laminar here based on the experimental data obtained with the Space Shuttle.[14] Calculation is performed only for the windward side of the airfoil and the blunt-nose region. Accurate calculation of the leeward side is not possible with the present code because the vibration model used is not valid for the expanding flow (see vibrational model). However, since the pressure in the leeward side is much smaller than the pressure in the windward side, the present calculation is expected to yield at least approximately the impact of real gas effects on the aerodynamic coefficients of the airfoil. The calculation is made with the two-temperature model and the perfect-gas model. A $131 \times 39 = 5109$-node grid is used for this calculation. The computing time for this case is 410 s for 700 iterations. The wall temperature is assumed to be 1500 K.

Figure 5 shows the distribution of atomic oxygen, atomic nitrogen, and nitric oxide mass fractions within the boundary layer at the (windward side) trailing edge. As seen in the figure, there are significant amounts of reaction products within the boundary layer. These are produced by the combination of the viscous dissipation (boundary-layer recovery phenomenon) and the blunt leading edge.

Because of these chemical reactions within the boundary layer, the boundary-layer displacement thickness becomes smaller. As a result, the shock envelope shrinks in the relaxing-gas flow. As Fig. 6 shows, the shock envelope is about 10% smaller in the relaxing-gas case compared with the perfect-gas case.

The shrinkage of the shock envelope accompanies the reduction of the shock angles. This in turn causes the postshock pressure to be smaller resulting ultimately in the reduction of the pressure at the wall. This phenomenon is demonstrated in Fig. 7 in which the pressure coefficient is plotted against the distance along the wall surface. The distance is measured from the trailing edge. As the figure shows, the relaxing gas produces generally lower pressures on the wall when compared with the perfect gas. In the figure, the wavy appearance of pressure for the perfect gas case at the distance of around 8 m is confirmed by examining the iteration-by-iteration evolution of the profile to be genuine: it is not due to the oscillation in the solution, but is believed to be due to the particular combination of γ and distribution of wall curvature for this case.

The pressure reduction seen in Fig. 7 is bound to affect the lift, drag, and pitching moment of the airfoil. In Fig. 8, the lift coefficient values, which include the skin friction effect, are compared between the two-temperature relaxing and the perfect-gas cases, as a function of the iteration number. As seen here, the computed lift coefficient values become approximately constant beyond about 400 iterations. At the iteration numbers of 700, the two lift coefficient values differ by about 10%: it is about 0.16 for the relaxing gas and 0.175 for the perfect gas. Between the iteration numbers of 400 and 700, the lift coefficient for the relaxing gas gradually increases. In order to confirm the convergence of the solutions, the calculation was carried to a total iteration number of 3000 for the relaxing gas. The result shows that there is virtually no change

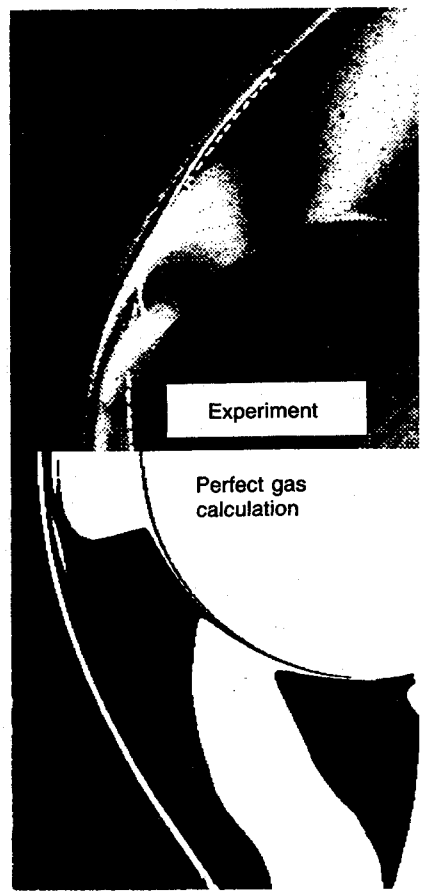

a) Calculation for perfect gas

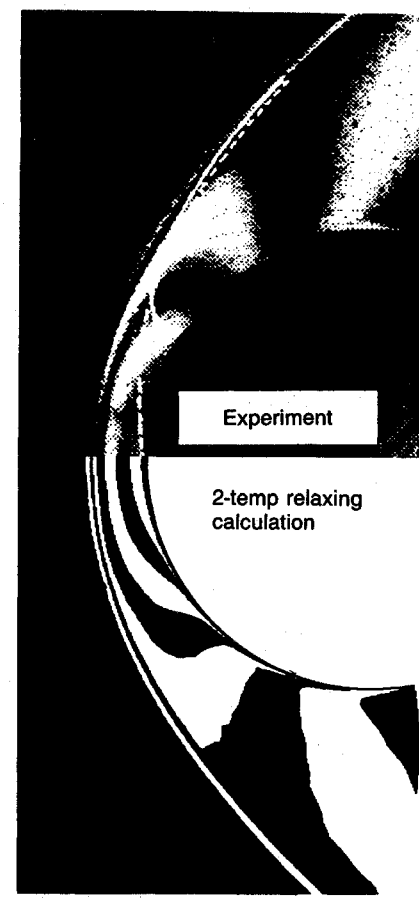

c) Calculation for two-temperature relaxing gas

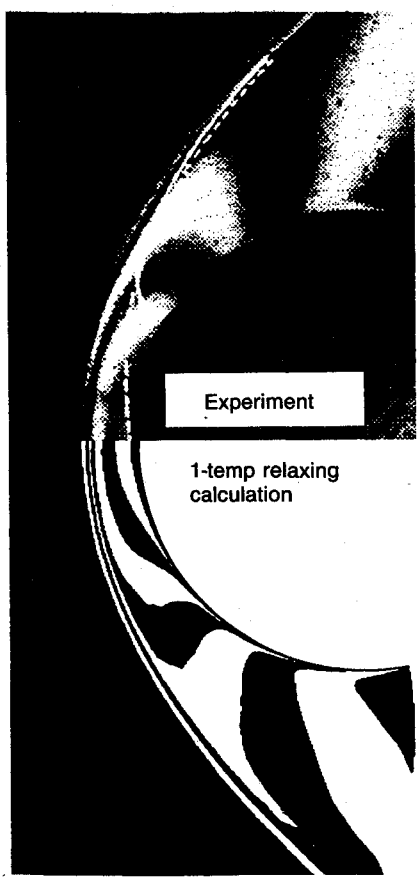

b) Calculation for one-temperature relaxing gas

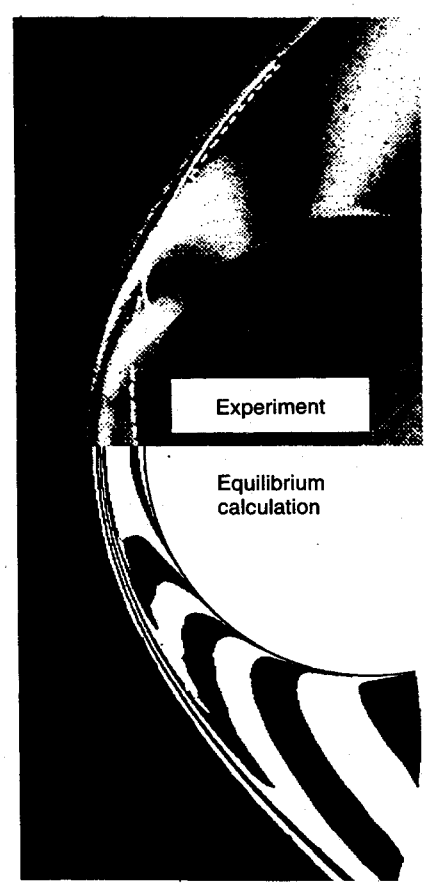

d) Calculation for equilibrium gas

Fig. 2 Comparison between the experimental[6] and computational interferograms for a flow around a circular cylinder of 2.54 cm radius; freestream conditions: $\rho = 5.35 \times 10^{-3}$ kg/m^3, velocity = 5.59 km/s.

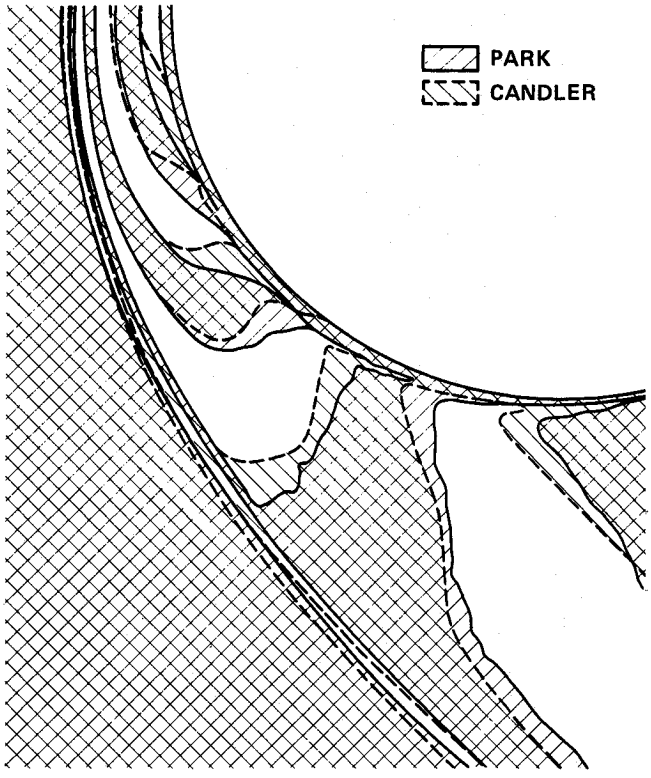

Fig. 3 Comparison between the present two-temperature calculation and multitemperature calculation by Candler.[5]

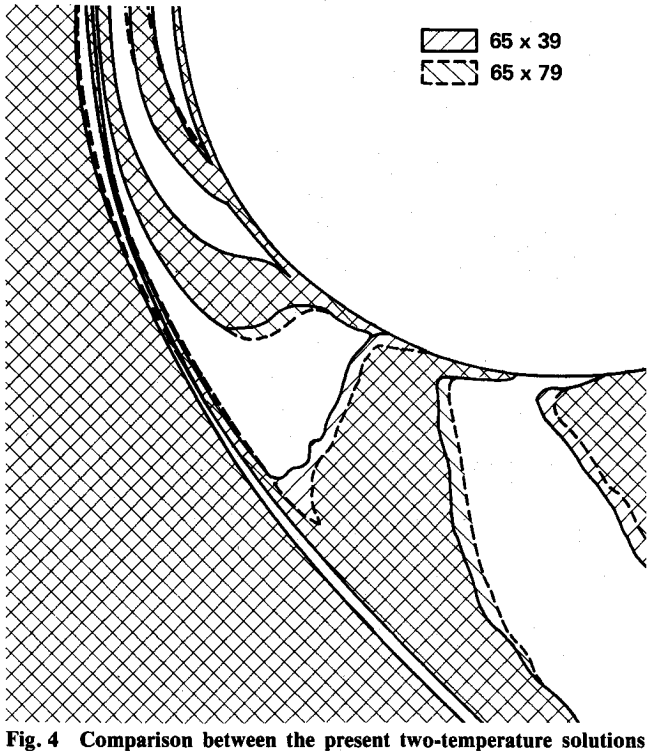

Fig. 4 Comparison between the present two-temperature solutions between 65×39 and 65×79 meshes.

in the lift coefficient beyond 700 iterations for the relaxing gas. The gradual increase between the iteration numbers of 400 and 700 is believed to be caused by the slow relaxation of the flow variables in the boundary layer, which is unrelated to the computational capability of the present code.

In Fig. 9, a similar comparison is made for the drag coefficient. The drag coefficient is about 0.076 for the two-temperature, relaxing-gas case and about 0.083 for the perfect-gas case—again about a 10% difference.

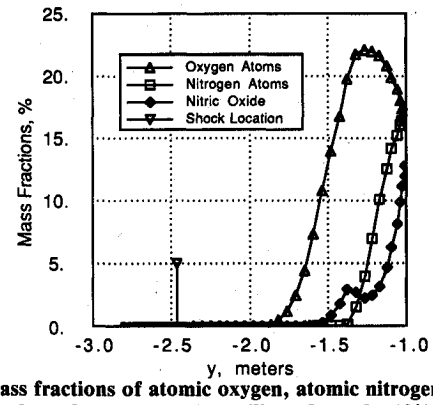

Fig. 5 Mass fractions of atomic oxygen, atomic nitrogen, and nitric oxide in the boundary layer at the trailing edges of a 10% half-elliptic airfoil. Chord length = 10 m, leading-edge radius = 10 cm.

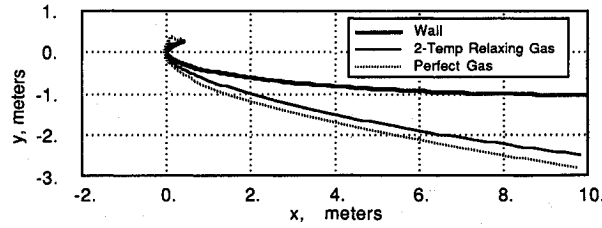

Fig. 6 Comparison of the shock shape over the 10% airfoil between the two-temperature relaxing-gas and the perfect-gas flows; flow conditions same as in Fig. 5.

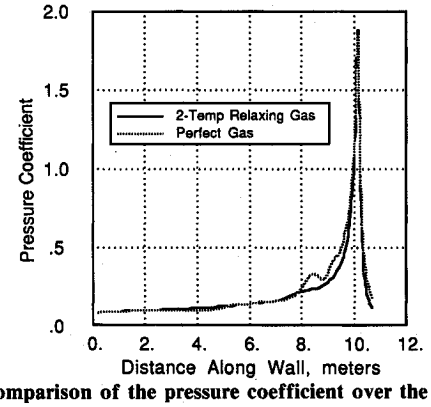

Fig. 7 Comparison of the pressure coefficient over the 10% airfoil between the two-temperature, relaxing-gas and the perfect-gas flows; flow conditions same as in Fig. 5.

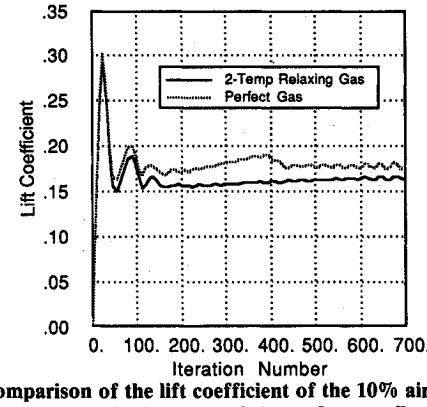

Fig. 8 Comparison of the lift coefficient of the 10% airfoil between the two-temperature relaxing-gas and the perfect-gas flows; flow conditions same as in Fig. 5.

In Fig. 10, a similar comparison is made for the pitching-moment coefficient taken around the chord midpoint. The chord midpoint is chosen for this calculation because it is the theoretical center of pressure for a Newtonian hypersonic flow for a flat plate. The moment coefficient is about 0.04 for the relaxing gas and 0.0049 for the perfect-gas case—a 20% difference.

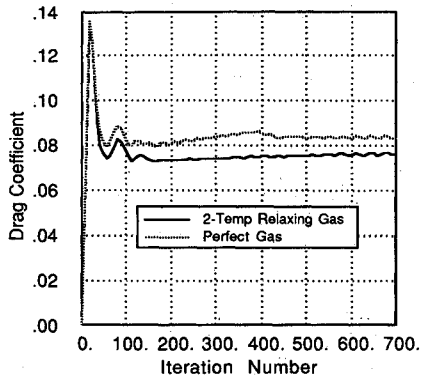

Fig. 9 Comparison of the drag coefficient of the 10% airfoil between the two temperature relaxing-gas and the perfect-gas flows; flow conditions same as in Fig. 5.

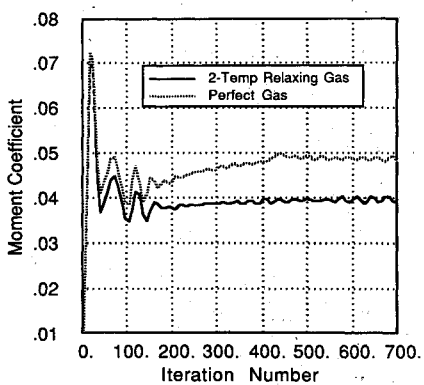

Fig. 10 Comparison of the pitching moment coefficient of the 10% airfoil between the two-temperature relaxing-gas and the perfect-gas flows; flow conditions same as in Fig. 5.

These results indicate the importance of the chemical reactions for an airfoil at a fairly small angle of attack. In order to accurately determine the aerodynamic coefficients, one must account for the thermochemical nonequilibrium phenomena correctly.

Conclusions

The CENS2H code developed for computing the thermochemical nonequilibrium flow in the suborbital flight speed range fully couples the phenomena with the fluid flow, is fully implicit, and converges within about 700 iterations. It takes 88 μs per node per iteration on a Cray X-MP computer. The calculation correctly reproduces the density distribution and the shock standoff distance for a cylinder in a dissociating nitrogen stream. For a 10%-thickness airfoil of chord length 10 m flying at an altitude of 55 km at Mach 20 at an angle of attack of 10 deg, the code predicts the lift and drag coefficients to deviate from the perfect-gas values by about 10% because of the thermochemical phenomena. For the pitching moment coefficient, the deviation is about 20%.

References

[1]Park, C., "Assessment of Two-Temperature Kinetic Model for Ionizing Air," *Journal of Thermophysics and Heat Transfer*, Vol. 3, No. 3, 1989, pp. 233–244.

[2]Candler, G. V., and MacCormack, R. W., "The Computation of Hypersonic Ionized Flows in Chemical and Thermal Nonequilibrium," AIAA Paper 88-0511, Jan. 1988.

[3]Park, C., and Yoon, S., "Calculation of Real-Gas Effects on Blunt-Body Trim Angles," AIAA Paper 89-0685, Jan. 1989.

[4]Park, C., "Assessment of Two-Temperature Kinetic Model for Dissociating and Weakly-Ionizing Nitrogen," *Journal of Thermophysics and Heat Transfer*, Vol. 2, No. 1, 1989, pp. 8–16.

[5]Candler, G. V., "On the Computation of Shock Shapes in Nonequilibrium Hypersonic Flows," AIAA Paper 89-0312, Jan. 1989.

[6]Hornung, H. G., "Non-Equilibrium Dissociating Nitrogen Flow over Spheres and Cylinders," *Journal of Fluid Mechanics*, Vol. 53, Pt. 1, May 1972, pp. 149–176.

[7]Millikan, R. C., and White, D. R., "Systematics of Vibrational Relaxation," *Journal of Chemical Physics*, Vol. 39, No. 12, 1963, pp. 3209–3213.

[8]Lee, J. H., "Basic Governing Equations for the Flight Regimes of Aeroassisted Orbital Transfer Vehicles," *Progress in Astronautics and Aeronautics: Thermal Design of Aeroassisted Orbital Transfer Vehicles*, Vol. 96, edited by H. F. Nelson, AIAA, New York, 1985, pp. 3–53.

[9]Park, C., "Two-Temperature Interpretation of Dissociation Rate Data for N_2 and O_2," AIAA Paper 88-0458, 1988.

[10]Monant, J. P., Hanson, R. K., and Kruger, C. H., "Shock Tube Determination of the Rate Coefficient for the Reaction $N_2+O \rightarrow NO+N$," *Proceedings of the 17th Symposium (International) on Combustion*, Combustion Institute, Pittsburgh, PA, 1978, pp. 543–552.

[11]Hanson, R. K., Flower, W. L., and Kruger, C. H., "Determination of the Rate Constant for the Reaction $O+NO \rightarrow N+O_2$," *Combustion Science and Technology*, Vol. 9, Nos. 3–4, 1974, pp. 79–86.

[12]Yoon, S., and Jameson, A., "An LU-SSOR Scheme for the Euler and Navier-Stokes Equations," AIAA Paper 87-0600, 1987.

[13]Yoon, S., and Kwak, D., "Artificial Dissipation Models for Hypersonic External Flow," AIAA Paper 88-3708, 1988.

[14]Romere, P. O., and Whitnah, A. M., "Space Shuttle Entry Longitudinal Aerodynamic Comparisons of Flights 1-4 with Preflight Predictions," *Shuttle Performance: Lessons Learned*, NASA CP-2283, 1983, pp. 283–307.

Clark H. Lewis
Associate Editor